Plane-based deformation analysis of railway tracks using airborne laser scanning data

Annelies VOORDENDAG[1,*], **David HAENER**[2], and **Andreas WIESER**[1]

[1] *Institute of Geodesy and Photogrammetry, ETH Zürich, Stefano-Franscini-Platz 5, 8093 Zurich, Switzerland, (annelies.voordendag@geod.baug.ethz.ch, andreas.wieser@geod.baug.ethz.ch)*

[2] *Swiss Federal Railways (SBB), Bern, Switzerland, (david.haener@sbb.ch)*

[*] *corresponding author*

Abstract

Early detection of changes in the ballast of railway tracks and timely maintenance are important to ensure a highly-available and affordable railway service. In this paper, we present a novel method utilizing point clouds to detect ballast problems and assess temporal changes of a track. We assume that consecutive sleepers locally approximate a plane, with deviations of the point cloud from this plane indicating ballast anomalies, and changes of the planes over time indicating deformations of the track. We demonstrate the method using airborne laser scanning data of a 430 m long part of a railway track in Switzerland. The results indicate areas with ballast problems through a high percentage of anomalies ($>30\,\%$ in some cases). Our method provides more, and more easily interpretable, information about track conditions than conventional point-cloud based deformation analysis, like M3C2. It is applicable to photogrammetric point clouds as well as point clouds from different LiDAR sensors and platforms. As such, it complements existing track inspection and monitoring approaches, and helps to improve railway infrastructure management.

Keywords: railway tracks, ballast, deformation monitoring, point clouds, ALS, M3C2

Received: 29th November 2024. Revised: 24th February 2025. Accepted: 25th February 2025.

1 Introduction

Effective monitoring of the ballast condition of railway tracks, coupled with timely maintenance, is essential to ensure the reliability, safety, and cost-efficiency of railway operations (Hoelzl, 2023). Early detection of degradation or shifts in the ballast can prevent severe infrastructure problems. By proactively addressing these issues, railway operators maintain continuous service, reduce operational costs, and extend the overall lifespan of the track system (Podofillini et al., 2006; Caetano and Teixeira, 2015; Hansmann et al., 2021).

Conventional methods for detecting changes in railway tracks focus primarily on the rails themselves, utilizing advanced diagnostic vehicles equipped with a variety of sensors and measurement systems (Hoelzl et al., 2022). The collected data are analyzed to identify potential faults or irregularities, and to plan maintenance interventions (e.g., Berggren et al., 2014). The required accuracies are at the mm- to sub-mm-level (Higgins and Liu, 2018), and diagnostic data are usually collected at regular intervals depending on the frequency of use of the track, e.g., every 2 to 6 months for tracks of the Swiss Federal Railways (SBB).

However, when it comes to the track ballast, i.e., the layer of crushed stone below and between the sleepers, which in turn support the rails (see Fig. 1 in Hoelzl et al. (2022) for terminology), detection methods are often less advanced. Inspection of ballast conditions in Switzerland typically relies on visual assessment or manual measurements performed during scheduled track checks. Inspectors assess factors such as the level of ballast degradation, ballast contamination, and the proper drainage and load distribution of the track (Hoelzl et al., 2023).

Still, these conventional methods are laborintensive, time-consuming, and do not provide accurate information on the volumetric changes of the ballast. However, such information would be particularly relevant both as an indicator of potential ballast subsidence, and as an input to calculate how much ballast needs to be transported to a specific location (e.g., in preparation for tamping work). By extending monitoring capabilities to the ballast layer, the railway industry can thus further optimize maintenance practices and enhance the overall health of the track infrastructure (Berggren et al., 2014; Sadeghi et al., 2018). Due to the size (20–65 mm diameter) and irregular shape of the stones forming the ballast (Guo et al., 2018), the accuracy of these observations can be an order of magnitude lower than that of the railway track measurements. However, the measurements should allow identification of deviations of the mean ballast surface on the order of a few cm between consecutive sleepers.

In this paper, we introduce a novel approach, intended to support track ballast management by indicating problems like emerging voids beneath sleepers, ballast flow, and excessive track settlement. This is done through an assessment of the local planarity of the track surface and deformation analysis between pairs of epochs using point clouds obtained from airborne laser scanning (ALS), e.g., Wehr and Lohr (1999). We approximate the track surface patch-wise by planes through the sleepers, calculate anomalies in terms of deviations from this plane, and analyze these anomalies as well as the changes of the planes over time.

We denote the part of a railway track to be analyzed as region of interest (ROI). Here, we assume that the ROI is symmetric to the axis of the track, has constant width, and comprises the top surface of the ballast, the sleepers, and the rails along a continuous section of a single track (Fig. 1). We treat adjacent multiple tracks and parting tracks at a switch as different ROIs, although it may be possible to extend the approach later for joint processing of adjacent tracks.

Monitoring and maintenance of railway tracks are relatively new application fields for point clouds. A review of related publications was recently given by Dekker et al. (2023). Wunderlich et al. (2016) classified point cloud-based approaches to deformation monitoring. Our proposal combines geometry-based and parameter-based assessment in a way

Figure 1. Example of an ROI (light blue box) and patches (dark blue boxes) with length l and width w for the proposed patch-based analysis. Background image: orthophoto 2020 (SBB).

similar to Yang et al. (2017) or Xu et al. (2018). Holst et al. (2014) and Holst and Kuhlmann (2016) have discussed the importance of the reference surfaces chosen for the analysis, and several authors propose free-form surfaces for point-cloud-based monitoring (e.g., Harmening and Neuner, 2015). However, the specific geometry of railway tracks allows us to keep the complexity low by using planes and patches.

The main novelties of our approach comprise (i) the capability to extract information on ballast conditions already from a single epoch of data, and (ii) the adaptation of a surface-based two-epoch monitoring approach to the specific conditions of railway tracks. The single-epoch analysis can help in early detection of problems such as ballast flow or voids emerging beneath sleepers. The two-epoch analysis can help to study the evolution of such problems and to detect others, e.g., inadequate bearing layers, deterioration of substructure, and excessive ballast attrition (Selig and Waters, 1994; Powrie and Pen, 2016). Additionally, changes in the location and geometric relation of consecutive sleepers are relevant as indicators of corresponding changes of the rails and thus of the track itself.

In Section 2 we provide a detailed description of the proposed method. We then demonstrate the application to a real-world data set (Sect. 3) provided by the SBB and show selected processing results (Sect. 4). We conclude with a brief discussion and an outlook for future work in Section 5.

2 Methods

The input point clouds of both epochs are assumed to be georeferenced to the same coordinate frame, and any possible horizontal track displacements or deformations are assumed to be small (a few cm, at most). The underlying coordinate reference system is compound, consisting of projected 2d coordinates (North, East) and height (Up).

The processing starts with the definition of patches, each of them containing a short segment of the track. Each patch is first processed separately for each epoch: the points belonging to the patch are extracted and classified as sleeper or non-sleeper points; a plane is fitted to the sleeper points, and indicators quantifying the deviations of all patch points from the plane are calculated. Indicators of deformation are then obtained by combining the per-epoch results. This comprises calculating the deviations of the points of the second epoch from the best-fit plane of the first, and the changes of the plane in terms of height and tilt. All these indicators are finally aggregated for the entire track.

2.1 Patch definition

The patches are defined in a Eulerian sense, i.e., they are fixed in space rather than moving with the track. The union of all patches $\mathscr{B}_i$, $i = 1, \ldots b$, should represent the whole ROI (see Sect. 1). Railway tracks have very small tilt, e.g., the gradient (longitudinal tilt) is less than 2.3 deg and the maximum superelevation (expressed as lateral tilt) less than 5.7 deg within the SBB rail network, so patches can be defined as polygons in 2d (North, East). Taking into account that also the curvature of the tracks is typically small, we propose to use rectangular patches of constant width w (equal to the width of the ROI) and constant length l, placed symmetrically to the horizontal projection of the track axis at constant intervals l along this axis (Fig. 1). Neglecting the small overlap and gaps that result in curved parts of the track, we consider these patches to be non-overlapping and their union equal to the entire ROI.

A reasonable choice of w and l depends on the desired information and quality, the geometry of the track, the resolution of the point cloud, and its uncertainty. While we leave a detailed analysis of these relations and a potential optimization of the size, shape, and overlap of the patches for future work, we recommend choosing w approximately the width of the sleepers; l should be large enough such that each patch covers several consecutive sleepers but small enough that the nominal ballast surface is nearly planar within each patch.

Typically, the coordinates of points along the nominal track axis are known to the railway operator, and the deviations of the actual track from the nominal one are small (a few cm, or less). The patch locations can then be calculated from available geospatial data, independent of the point clouds. If no such data are available, or the deviations between nominal and actual track are too large, the point clouds must be collected with a sufficiently high resolution to facilitate automated extraction of the track axis from the point clouds, e.g., following Kononen et al. (2024) or Karunathilake et al. (2020). Due to the Eulerian approach taken herein, it is sufficient to do this for one of the epochs only.

2.2 Sleeper detection

Let $\mathbb{P}^k$, $k \in \{1,2\}$ be the point clouds of the two epochs, and $\mathbb{P}_i^k$ their subsets comprising all points whose horizontal coordinates are within patch $\mathscr{B}_i$. For the subsequent analysis, the points on sleepers, i.e., $\mathbb{S}_i^k \subset \mathbb{P}_i^k$ need to be extracted through an appropriate classification. It is beyond the scope of this paper to study which data and which classifier are best suited. Within this paper, we apply a handcrafted classifier which is sufficient for the specific sleepers present in our case study while it would likely fail with other tracks or other types of sleepers. It classifies points as sleeper points if their intensity is between the 15-th and 40-th percentile of the empirical distribution of all intensities within the respective patch. We carry out the classification separately for $\mathbb{S}_i^1$ and $\mathbb{S}_i^2$.

2.3 Plane fitting

For each patch and epoch, a plane π_i^k is fitted to the sleeper points $\mathbb{S}_i^k$. However, the real surface of individual sleepers is typically not a plane, consecutive sleepers are not necessarily parallel, and the sleeper classification will not be perfect. We thus propose to use a robust estimator for calculating the parameters of the planes and to ignore points within the point cloud which are farther than a certain threshold θ_π from the plane. Additionally, the estimation process should provide means to quantify the uncertainty of the results such that it can be taken into account for the assessment of deviations and deformations.

Within this paper, we use RANSAC (Fischler and Bolles, 1981) with a user-selected, fixed inlier threshold θ_π to estimate the normal vector and an offset per plane. We apply an approach inspired by bootstrapping, see e.g., Efron (1979), Neuner et al. (2014), or Kargoll et al. (2019), to estimate the covariance matrix of the parameters by repeating the estimation $N = 100$ times and calculating the empirical diagonal covariance matrix from the N estimation results. This data driven approach avoids the challenges of computing an appropriate, fully populated covariance matrix of the point cloud coordinates starting from assumptions (Kauker and Schwieger, 2016, 2017), and at the same time avoids the detrimental impacts of an over-simplified stochastic model (Zhao et al., 2019).

2.4 Patch-wise indicators

We interpret the orthogonal distances $\Delta z^k_{i,j}$ of the individual points j from the plane π^k_i as anomalies if their magnitude exceeds θ_π. Let the number of such anomalous points be $N^k_{i,a}$, and the total number of points, i.e., the number of all points of the corresponding patch and epoch, be $N^k_{i,t}$. If w is significantly smaller than the track gauge, and θ_π is large enough, anomalies calculated for a track in perfect shape should mostly be quasi-random consequences of the granular composition of the ballast and thus of the fact that the ballast surface is rough. A high percentage

$$P^k_{i,a} := 100 \times N^k_{i,a}/N^k_{i,t} \tag{1}$$

of anomalous points would indicate potential ballast problems in such a case.

If points on the rails or rail fasteners are part of the patches, e.g., because rails pass diagonally through a track near a switch or crossing, or because w is too large, and if these points are not removed before the analysis, then they will likely show up as anomalies (unless θ_π were chosen larger than the height of the fasteners and rails). However, also in this case, the percentage of anomalous points will typically be low if the track is in good shape. So, overall, the percentage $P^k_{i,a}$ of anomalies is an indicator of (geometric) ballast conditions.

In order to properly assess the deviations of the track surface from a plane, it is helpful to quantify the anomalies in addition to counting them. As a first step, we propose to do this by calculating the mean value of the positive anomalies and the mean value of the negative ones:

$$\Delta\bar{z}^k_{i+} := \frac{\sum_j \big(\Delta z_j \cdot I(\Delta z_j > \theta_\pi)\big)}{\sum_j I(\Delta z_j > \theta_\pi)}, \tag{2}$$

$$\Delta\bar{z}^k_{i-} := \frac{\sum_j \big(\Delta z_j \cdot I(\Delta z_j < -\theta_\pi)\big)}{\sum_j I(\Delta z_j < -\theta_\pi)}, \tag{3}$$

where $I(\cdot)$ is a function evaluating to 1 if the argument is true, and to 0 otherwise.

2.5 Indicators of deformation

Track deformations can be identified by comparing the point clouds from different epochs. The patch-based approach presented herein allows to perform the deformation analysis according to two of the approaches summarized by Wunderlich et al. (2016): a parameter-based deformation analysis focusing on the changes of the best-fit planes between the epochs, and a point cloud-based analysis focusing on the deviations of the points of one epoch from the best-fit plane of the other epoch. We restrict the analysis to approximately vertical components of deformation and displacement, corresponding to the high sensitivity of ALS data in the line-of-sight direction and of plane-based quantities in the direction perpendicular to the plane.

For the comparison of plane parameters, assume that the normal vector $\mathbf{n}$ has been estimated for each patch and epoch (i and k omitted here for simplicity) as a unit vector and is parameterized in terms of North, East and Up components with respect to the superordinate coordinate system, i.e.,

$$\mathbf{n} := \begin{bmatrix} n_N \\ n_E \\ n_U \end{bmatrix}, \quad ||\mathbf{n}|| = 1. \tag{4}$$

Additionally, let the azimuth of the track axis within the respective patch be t. Then, the longitudinal and lateral tilt, ν and ϕ, can be calculated for the respective patch and epoch from

$$\nu = \arctan \frac{-n_N \cos t - n_E \sin t}{n_U}, \tag{5}$$

$$\phi = \arcsin(n_N \sin t - n_E \cos t), \tag{6}$$

where $\nu > 0$ indicates rising track in the direction t, $\phi > 0$ indicates that the left hand rail is higher than the right hand rail as seen in direction t, and both angles are small enough for real tracks such that Eqs. (5) and (6) are unambiguous. Variance propagation from the covariance matrix of $\mathbf{n}$ to ν and ϕ allows to derive their standard deviations and subsequently assess the significance of the tilt changes between the epochs.

To assess potential height changes of the track, we intersect the planes fitted for the two epochs with a vertical line through the center $\mathbf{C} := [C_N, C_E, C_U]$ of the patch. The height value of the intersection points is obtained from the components of the normal vector, the coordinates of $\mathbf{C}$, and the plane's distance d from the origin as

$$U_\pi = \frac{1}{n_U} \cdot (d - n_N C_N - n_E C_E). \tag{7}$$

Based on all above assumptions and the choice of rectangular patches symmetric about the track axis (Sect. 2.1), the height difference between these two points represents the height change of the track sufficiently well. Again, variance propagation allows to calculate also the standard deviations of the heights and use those for statistical significance testing.

Finally, for the point-cloud-based analysis, we calculate the anomalies of the patch points $\mathbb{P}_i^2$ of the second epoch with respect to the best-fit plane π_i^1 of the first epoch, and derive the indicators introduced in Section 2.4 also for this case.

2.6 Track assessment

For assessing the track ballast conditions and deformations, we aggregate the patch-based analysis results over the whole track.

Currently, this consists of plotting the indicator values versus stationing along track. Closer visual inspection of segments with irregular indicators helps to identify potentially problematic parts of the track, and the indicators can be used by experts to further investigate the track conditions and plan appropriate counter measures. We see this visual inspection as a first step towards a more automated point-cloud-supported track assessment, but leave the development of the related algorithms, possibly comprising machine learning, for the future.

3 Study site and data

We demonstrate the application of the method using ALS data from a 430 m long part of a railway track in Switzerland (Fig. 2), acquired in December 2016 and March 2020. The sleepers are approximately 2.6 m wide in this area, and therefore we define the ROI of the analysis as the area symmetrically extending 1.3 m from both sides of the nominal track axis. This axis was available from a database as coordinates of points approximately 4 m apart.

The ALS data were collected from a helicopter, and processed into georeferenced point clouds in the Swiss coordinate frames LV95 (projected coordinates) and LN02 (height) by an external company. The data acquisition was not custom-tailored to the present study but had been designed for an assessment of the ground movements along the railway track. Relevant details of the data acquisition and data set can be found in Table 1.

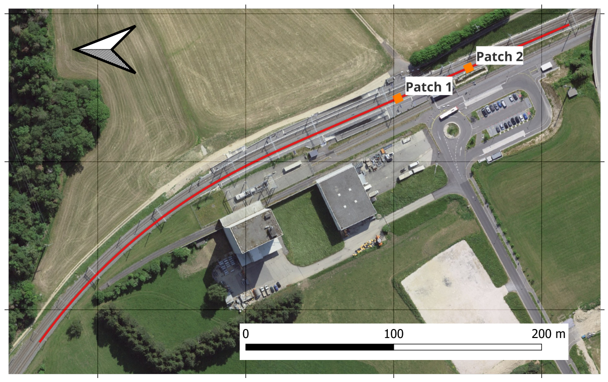

Figure 2. Study site in Switzerland with two patches (orange markers) indicated on the analyzed railway track (red line, 430 m long). Background image: swisstopo.

Table 1. Key parameters of data acquisition and point clouds used within this study (source: SBB)

Parameter (unit)	2016 / 2020
Flight altitude (m)	170 / 240
LiDAR sensor	Riegl VQ480U / Riegl VQ480ii
Pulse repetition rate (kHz)	550 / 2000
Point density (pts m^{-2})	approx. 140 / 230
Width covered per pass (m)	170 / 360
Accuracy (1σ, elev.) (cm)	3–5 / 3–5
Accuracy (1σ, horiz.) (cm)	5 / 3–5

4 Results

According to the width of the ROI, we used $w = 2.6$ m for the rectangular patches. For convenience, we chose a length $l \approx 4$ m without an underlying optimization or analysis of deformations to be expected. This choice assured that we could directly tie the rectangular patches to the given track axis points, and still had at least 6 sleepers and >500 scanned points for defining the plane per patch. Taking into account the noise and vertical accuracy of the scan data (Table 1), we chose a threshold $\theta_\pi = 3$ cm for plane estimation and anomaly detection.

Figure 3 shows the anomalies calculated according to Sections 2.4 and 2.5 for two patches. We also include deformation magnitudes from a conventional M3C2 analysis (Lague et al., 2013) for comparison.

Patch 1 comprises about 2400 points in epoch 1 (2016) and 5000 in epoch 2 (2020). There are only $P_{1,a}^{2016} = 20\%$ and $P_{1,a}^{2020} = 13\%$ of anomalous points, with the majority of the positive anomalies representing the rails (Figs. 3a, 3c). The few other ones are small and mostly correspond to isolated points at the ballast between the sleepers. These anomalies do thus not indicate any ballast problems.

The situation is different for patch 2, where $P_{2,a}^{2016} = 32\%$ of the points are anomalous in epoch 1, with a clearly visible excess of ballast (anomalies up to about 20 cm) along the western (bottom) side of the patch and ballast covering the sleepers in that region (Fig. 3e). This may indicate a ballast flow problem. Much of this excess ballast has apparently been removed between epochs 1 and 2, (Fig. 3g), where $P_{2,a}^{2020}$ is down to 17% and most anomalies are again related to the rails.

The anomalies of epoch 2 with respect to the plane from epoch 1 (Figs. 3b, 3f) indicate deformation of the ballast surface between the epochs, for both patches. In this case, we identify 25% and 32% of the points as anomalies for patches 1 and 2, respectively. Some increase in anomalies is expected, as compared to the analysis using the plane from the same epoch; georeferencing errors affect any type of between-epoch deformation analysis. Still, the changes mostly relate to the ballast while the sleepers themselves have not changed by more than $\theta_\pi = 3$ cm. In fact, the planes change only by $\Delta U_{1,\pi} = -7$ mm and $\Delta U_{2,\pi} = -18$ mm for the two patches, respectively, see Fig. 4e. These changes could be seen as indicating subsidence of the sleepers or consequences of track maintenance, but the accuracy of the georeferencing (3 to 5 cm) is too low to draw such a conclusion.

The established M3C2 analysis (Figs. 3d, 3h) shows on average only a slight subsidence but virtually no changes by more than 3 cm for patch 1, which agrees well with the above results. However, the M3C2 results indicate a clear subsidence of the surface for the part of patch 2, which is hard to correctly interpret as removal of excess ballast rather than subsidence of the track.

Figure 4 shows several of the patch-wise indicators, aggregated according to Section 2.6. Across the whole track, i.e., for all patches, there are between 12 and 55% of anomalies. Based on the nominal cross section of the rails and the size/arrangement of the sleepers in the study area we assume that 6% of the points per patch are rail points more than $\theta_\pi = 3$ cm above the sleepers. So, in our case, the rails account for a minimum of 6% (positively) anomalous points. Scanning noise and ballast roughness also result in detected anomalies with the given value of θ_π. Taking into account the above analysis of patches 1 and 2 as well as the lowest percentages in Figure 4a, we assume that values below 20% indicate a track with ballast in excellent geometric conditions, whereas values higher than 30% indicate likely ballast distribution problems.

Applying these thresholds, Figure 4a indicates that (i) the ballast distribution was likely problematic in 2016 for some areas around 50 m chainage (distance along track) and between 100 and 170 m, (ii) the ballast distribution has changed significantly in several parts of the track, especially from about 280 m to the end, and (iii) the ballast showed minimal anomalies from the plane in 2020 for most of the track, except the final 70 m. Indeed, there has been track maintenance between the two epochs, which explains the improvements, and the ROI ends at a section with a rail crossing and a buffer stop, where, on the one hand, additional infrastructure on the track affects the anomaly assessment, and on the other hand, the ballast distribution does not need to have the same high quality as along other parts of the track.

The lateral tilt ϕ (Fig. 4b) is related to track curvature and corresponds qualitatively to the expectation. It is up to almost 5 deg in the curve and around

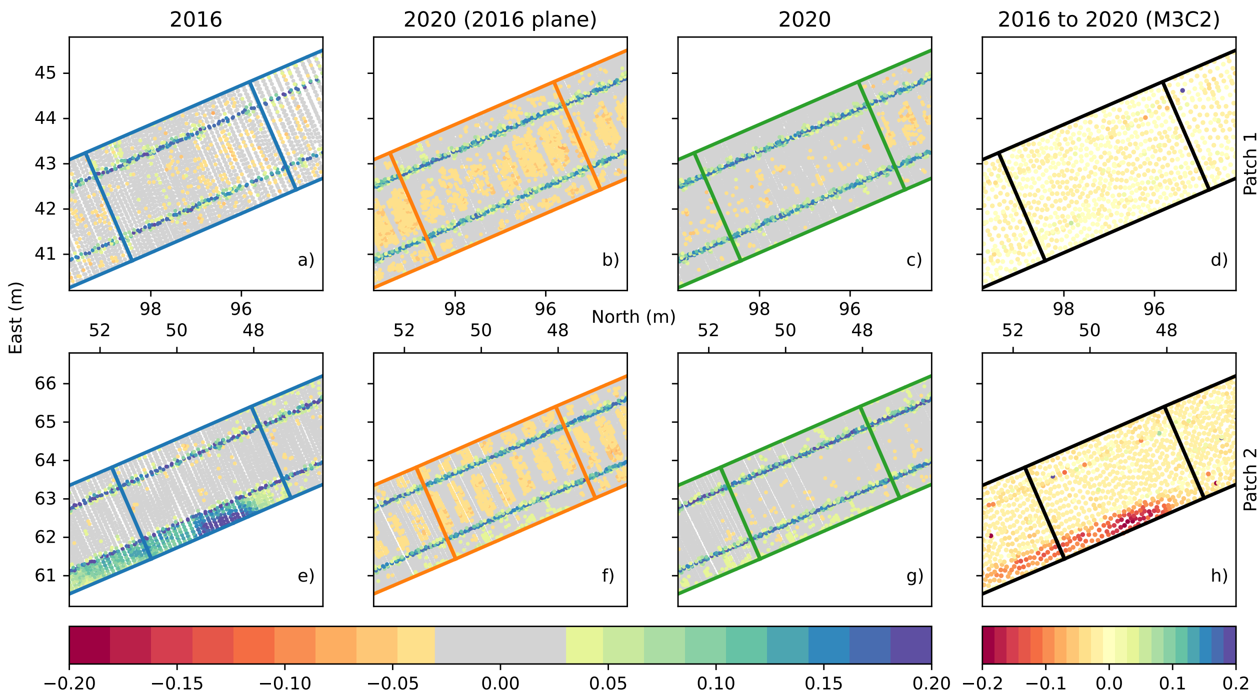

Figure 3. a)-c) Patch of the point cloud (colored box) with the points on the plane (0±0.03 m, grey) and anomalies (colors). a) denotes the point cloud and plane from 2016, b) is the plane from 2016 with point cloud from 2020, and c) the point cloud and plane from 2020. d) M3C2 deformation analysis between 2016 and 2020. e) to h) are the same, but for patch 2 (see Fig. 2) of the track. The color bars denote the anomalies from the planes and M3C2 distances, respectively, in m. Note that the axes are turned 90° conforming to Figure 2.

0 in its straight section with apparent greater variability in some parts of the curve and towards the buffer stop at the end. The standard deviations of the tilt values, extracted from the point cloud, are on the order of 0.1 deg, corresponding to 3.3 mm for the superelevation.

We do not display the longitudinal tilt v here, as the estimates were non-significant due to the low gradient (about 0.6 m height change over the entire ROI, i.e., less than 1.5‰ or 0.06 deg) and standard deviation of about 0.08 deg of the estimates.

Like the percentages (Fig. 4a), the average positive anomalies (Fig. 4c) include the rails and are thus biased. Figure 4c indicates some patches with much higher values than the surrounding ones. This may point at actual ballast problems, as e.g., for patch 2 (see above). However, the values are difficult to interpret, because they are mostly around 0.10 m while the height of the rails is about 0.17 m, and excellent ballast conditions could result both in mean positive anomalies close to 0.17 m (if the rails are the only anomalies) or much lower values (if the ballast surface is at nearly the same height as the sleepers, and scanning noise and ballast roughness result in a relatively large number of small positive anomalies). We leave it for future work to solve this problem by improved segmentation of the point clouds such that rails and ballast can be distinguished in the analysis.

The mean negative anomalies (Fig. 4d) are not affected by the rails. Most of them are around 0.04 m and are dominated by the impact of ballast particle size and scanning noise. Only the strikingly lower values towards the end of the track clearly indicate that there may be areas with a lack of ballast or poor ballast distribution, requiring closer inspection. Figure 4d also shows that our method is applicable to railway tracks where the ballast is in general lower than the sleeper surfaces, as there is always a certain amount of negative anomalies. However, future developments of the algorithm may allow offsetting the planes by a nominal amount along their normal vectors before calculating anomalies. This will better accomodate situations, where the nominal bal-

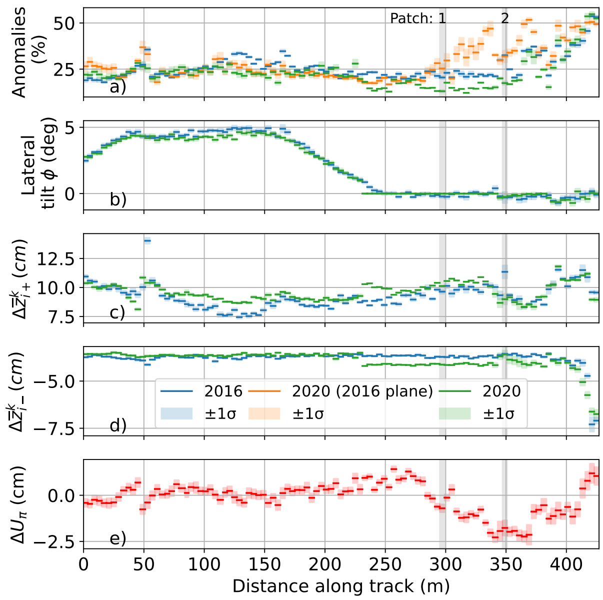

Figure 4. a) Percentage of anomalies from the derived plane with a threshold distance to the plane of 0.03 m for the 2016 data (blue), the 2020 data with the plane equation of 2016 (orange) and the 2020 with a new derived plane (green) for each patch. b) Lateral tilt ϕ. c) Average anomaly of all anomalies above the plane. d) Average anomaly of all anomalies below the plane. e) The height difference between 2016 and 2020 of the center points of each patch. Patch 1 and 2 from Figure 3 are indicated with grey bars.

last surface does not coincide with the envelope of the sleepers.

Last, the height changes ΔU_π (Fig. 4e) of the planes between 2016 and 2020, representing the patch-wise estimates of the height changes of the sleepers and thus rails, overall indicate only small changes except for the last about 150 m of the track, where the track has been lowered by up to 2 cm. Considering the standard deviations of the estimated values, the underlying real height changes are likely smooth along the track except for very few locations (e.g., around 50, 260 or 340 m), which might need a closer inspection. The accuracy of these estimates is affected by the uncertainty of the point cloud registration and georeferencing, potentially resulting in some long-wavelength biases of the estimated values ΔU_π. Further research is needed to properly quantify those and take them into account for the assessment of the results.

5 Discussion and conclusion

The method presented in this study supports the monitoring of railway tracks with a focus on assessing geometric ballast conditions. As a point-cloud based method it allows combining documentation with a variety of quantitative analyses. The underlying assumptions are that (i) the surface of consecutive sleepers approximate a plane sufficiently well, (ii) changes of this plane over time correspond to changes of the rails and track, (iii) significant deviations of points of the track surface from this plane (except the rails) indicate potential ballast problems, (iv) the point cloud data contain a sufficient number of points from the surface of the sleepers, and (v) the point clouds are correctly segmented into sleeper and non-sleeper points.

In our view, a key strength of the proposed method, and an advantage over established point-cloud deformation analysis approaches like M3C2, is that it allows assessing the state of the track ballast even with scan data from a single epoch or with different data acquisition parameters between epochs. Additionally, the results may be easier to interpret than standard point cloud differences. Although this method can only complement and not replace regular track diagnosis (which requires determining the geometry of the loaded track with very high accuracy), it may help railway operators detect problems and plan maintenance measures early. Furthermore, it may help to gain a better understanding of certain phenomena (e.g., voids beneath sleepers, or ballast flow). We anticipate that ballast scans might be most useful if carried out once or a few times between consecutive diagnostic surveys, i.e., once per 4 to 12 weeks within SBB's network, depending on the use and conditions of the track.

The study case presented in Sections 3 and 4 served to demonstrate the main ideas of the approach, provide an impression of its potential benefits, and identify needs for further research. We have identified several points for potential improvement and necessary further investigations by ourselves and others. One of these areas is the point cloud segmentation, which should be versatile enough to correctly identify (i) sleeper points and (ii) rail points for all relevant track configurations (material and shape of the sleepers, distance between sleepers, type and conditions of ballast, crossings and switches); this can be based on point cloud geometry and intensities, but may also have to include RGB images or even prior knowledge about the track. Another area requiring further research is the optimum choice of patch shape, patch size, thresholds for calculation and interpretation, as well as their relation to ballast chip size, point cloud noise, and other potentially relevant parameters. Finally, it will be required to automate the joint assessment of the point-cloud based results, possibly in combination with image analysis, and to classify identified track problems or confirmation of good track conditions in a way to support planning and operation of network maintenance.

Herein, we only used ALS data. However, the algorithms proposed are agnostic regarding the source of the point clouds, and we anticipate that it will be possible to apply them to data from e.g., airborne photogrammetry, UAV-based photogrammetry, UAV-based LiDAR, or train-based LiDAR. The plane-based approach and the proposed indicators allow a comparison between epochs even if the data have been acquired with different acquisition parameters (Table 1) or even with different point cloud sensor technologies and platforms. This may facilitate efficient data acquisition and quality assurance in the future by combining data from track inspection with a diagnostic vehicle and fully autonomous UAV flights. With this flexibility and the potential to provide relevant information with high technical quality and operational efficiency, we expect the proposed method to be a foundation for future, automated railway track ballast monitoring contributing to enhanced railway infrastructure management.

Acknowledgements

This research was supported by AMAG, Siemens Mobility and SBB through an ETH Mobility Initiative grant (”REASSESS”). Nicolas Ackermann (SBB) provided the point cloud data. The implementation of the sleeper detection and the comments regarding rail detection were inspired by a student project (Philippe Bättig, Julian Bleiker Chiara Sabato). The M3C2 analysis was provided by Pia Ruttner and Nicholas Meyer. We used ChatGPT for initial language editing of some parts and for coding (Python), but we take full responsibility for content, language and appearance of the paper.

References

Berggren, E. G., Nissen, A., and Paulsson, B. S. (2014). Track deflection and stiffness measurements from a track recording car. *Proc. Inst. Mech. Eng., Part F: J. Rail Rapid Transit*, 228(6):570–580.

Caetano, L. F. and Teixeira, P. F. (2015). Optimisation model to schedule railway track renewal operations: a life-cycle cost approach. *Struct. Infrastruct. E.*, 11(11):1524–1536.

Dekker, B., Ton, B., Meijer, J., Bouali, N., Linssen, J., and Ahmed, F. (2023). Point cloud analysis of railway infrastructure: A systematic literature review. *IEEE Access*, 11:134355–134373.

Efron, B. (1979). Bootstrap methods: Another look at the jackknife. *Ann. Statist.*, 7(1):1–26.

Fischler, M. A. and Bolles, R. C. (1981). Random sample consensus: a paradigm for model fitting with applications to image analysis and automated cartography. *Commun. ACM*, 24(6):381–395.

Guo, Y., Markine, V., Song, J., and Jing, G. (2018). Ballast degradation: Effect of particle size and shape using los angeles abrasion test and image analysis. *Construction and Building Materials*, 169:414–424.

Hansmann, F., Nemetz, W., and Spoors, R. (2021). *Keeping track of track geometry*. PMC Media House GmbH.

Harmening, C. and Neuner, H. (2015). Continuous modelling of point clouds by means of freeform surfaces. *Vermessung & Geoinformation*, 103:121–129.

Higgins, C. and Liu, X. (2018). Modeling of track geometry degradation and decisions on safety and maintenance: A literature review and possible future research directions. *Proceedings of the Institution of Mechanical Engineers, Part F: Journal of Rail and Rapid Transit*, 232(5):1385–1397.

Hoelzl, C. (2023). *On board monitoring for railway infrastructure condition assessment*. PhD thesis, ETH Zurich.

Hoelzl, C., Arcieri, G., Ancu, L., Banaszak, S., Kollros, A., Dertimanis, V., and Chatzi, E.

(2023). Fusing expert knowledge with monitoring data for condition assessment of railway welds. *Sensors*, 23(5):2672.

Hoelzl, C., Dertimanis, V., Landgraf, M., Ancu, L., Zurkirchen, M., and Chatzi, E. (2022). *Chapter 9 - On-board monitoring for smart assessment of railway infrastructure: A systematic review*, pages 223–259. Elsevier.

Holst, C., Artz, T., and Kuhlmann, H. (2014). Biased and unbiased estimates based on laser scans of surfaces with unknown deformations. *Journal of Applied Geodesy*, 8:169–183.

Holst, C. and Kuhlmann, H. (2016). Challenges and present fields of action at laser scanner based deformation analyses. *Journal of Applied Geodesy*, 10:17–25.

Kargoll, B., Omidalizarandi, M., Paffenholz, J.-A., Neumann, I., Kermarrec, G., and Alkhatib, H. (2019). Bootstrap tests for model selection in robust vibration analysis of oscillating structures. In *Proc. 4th Joint International Symposium on Deformation Monitoring (JISDM)*.

Karunathilake, A., Honma, R., and Niina, Y. (2020). Self-organized model fitting method for railway structures monitoring using lidar point cloud. *Remote Sensing*, 12:1–15.

Kauker, S. and Schwieger, V. (2016). First investigations for a synthetic covariance matrix for monitoring by terrestrial laser scanning. In *Proc. 3rd Joint International Symposium on Deformation Monitoring (JISDM)*, pages 1–10.

Kauker, S. and Schwieger, V. (2017). A synthetic covariance matrix for monitoring by terrestrial laser scanning. In *Journal of Applied Geodesy*, volume 11, pages 77–87. Walter de Gruyter GmbH.

Kononen, A., Kaartinen, H., Kukko, A., Lehtomäki, M., Taher, J., and Hyyppä, J. (2024). Fully automated extraction of railtop centerline from mobile laser scanning data. *Automat. Constr.*, 168:105812.

Lague, D., Brodu, N., and Leroux, J. (2013). Accurate 3D comparison of complex topography with terrestrial laser scanner: Application to the Rangitikei canyon (N-Z). *ISPRS J. Photogramm. Remote Sens.*, 82:10–26.

Neuner, H., Wieser, A., and Krähenbühl, N. (2014). Bootstrapping: Moderne Werkzeuge für die Erstellung von Konfidenzintervallen. In *DVW Schriftenreihe*, volume 74, pages 151 – 170.

Podofillini, L., Zio, E., and Vatn, J. (2006). Risk-informed optimisation of railway tracks inspection and maintenance procedures. *Reliab. Eng. Syst. Safe.*, 91(1):20–35.

Powrie, W. and Pen, L. (2016). *A Guide to Track Stiffness*. University of Southampton Department of Civil & Enviromental Engineering.

Sadeghi, J., Motieyan-Najar, M. E., Zakeri, J. A., Yousefi, B., and Mollazadeh, M. (2018). Improvement of railway ballast maintenance approach, incorporating ballast geometry and fouling conditions. *J. Appl. Geophys.*, 151:263–273.

Selig, E. T. and Waters, J. M. (1994). *Track geotechnology and substructure management*. Thomas Telford Publishing.

Wehr, A. and Lohr, U. (1999). Airborne laser scanning—an introduction and overview. *ISPRS J. Photogramm. Remote Sens.*, 54(2–3):68–82.

Wunderlich, T., Niemeier, W., Wujanz, D., Holst, C., Neitzel, F., and Kuhlmann, H. (2016). Areal deformation analysis from tls point clouds-the challenge. *AVN*, 123:340–351.

Xu, X., Yang, H., and Neumann, I. (2018). A feature extraction method for deformation analysis of large-scale composite structures based on tls measurement. *Composite Structures*, 184:591–596.

Yang, H., Omidalizarandi, M., Xu, X., and Neumann, I. (2017). Terrestrial laser scanning technology for deformation monitoring and surface modeling of arch structures. *Composite Structures*, 169:173–179.

Zhao, X., Kermarrec, G., Kargoll, B., Alkhatib, H., and Neumann, I. (2019). Influence of the simplified stochastic model of tls measurements on geometry-based deformation analysis. *Journal of Applied Geodesy*, 13:199–214.